Journal of
Polymer Materials

Tech Science Press

https://doi.org/10.32604/jpm.2026.077915

ARTICLE

Electrical, Structural, and Electronic Insights of Polysaccharide-Based Biopolymer Electrolytes Incorporated with Sodium Perchlorate Salt

Rabiatul Akashah Rusli[1], Siti Zafirah Zainal Abidin[1,2,*], Nur Farisha Sulthan Hussain[1] and Siti Rudhziah Che Balian[3]

[1]Faculty of Applied Sciences, Universiti Teknologi MARA, Shah Alam, Selangor, Malaysia
[2]Ionic Materials and Devices (iMADE) Research Laboratory, Institute of Science, Universiti Teknologi MARA, Shah Alam, Selangor, Malaysia
[3]Centre of Foundation Studies, Universiti Teknologi MARA, Cawangan Selangor, Kampus Dengkil, Dengkil, Selangor, Malaysia

*Corresponding Author: Siti Zafirah Zainal Abidin. Email: szafirah@uitm.edu.my

Received: 19 December 2025; Accepted: 26 February 2026; Published: 30 June 2026

ABSTRACT: The urgent demand for sustainable energy materials aligned with the United Nations Sustainable Development Goal 7 has intensified interest in biopolymer electrolytes (BPEs). Many non-polysaccharide biopolymers exhibit low ionic conductivity and weak salt dissociation at room temperature, limiting their performance in sodium-ion energy storage devices. Polysaccharides such as guar gum provide abundant coordination sites that can enhance Na^+ transport. This study investigates the electrical, structural, and electronic behaviour of guar gum–sodium perchlorate (guar gum–$NaClO_4$) BPEs to establish structure–transport relationships. Biopolymer electrolyte films were prepared via solution casting using guar gum (0.5 g) with $NaClO_4$ at six salt loadings: 0, 10, 20, 30, 40, and 50 wt.%. Electrochemical impedance spectroscopy (EIS) was conducted at room temperature for all compositions and at elevated temperatures (303–343 K) for selected samples (0, 30, and 40 wt.%). Structural properties were examined by X-ray diffraction (XRD), and crystallite size was quantified using the Scherrer equation. Electronic properties, including density of states (DOS) and frontier molecular orbitals, were evaluated using density functional theory (DFT) with the DMol^3 module. Ionic conductivity increased from 9.13×10^{-9} S·cm^{-1} in the unadded salt guar gum sample (0 wt.%) to a maximum of 8.40×10^{-4} S·cm^{-1} at 40 wt.% $NaClO_4$, attributed to enhanced $NaClO_4$ dissociation and reduced bulk resistance. At 50 wt.%, conductivity decreased to 3.37×10^{-4} S·cm^{-1}, indicating ion pairing. Temperature-dependent EIS confirmed Arrhenius behaviour, with the 40 wt.% sample exhibiting the lowest activation energy (7.61×10^{-20} eV). XRD analysis showed progressive amorphization with crystallite size reducing from 5.05 nm (0 wt.%) to 0.82 nm (40 wt.%), correlating with enhanced ionic mobility. DFT findings revealed strong guar gum–$NaClO_4$ interactions and a significant HOMO–LUMO band-gap reduction from 6.6129 eV (unadded salt guar gum) to 0.3813 eV, suggesting improved electronic flexibility and salt dissociation. The combined EIS, XRD, and DFT analyses demonstrate that guar gum–$NaClO_4$ BPEs exhibit strong structure–transport coupling, with 40 wt.% $NaClO_4$ producing optimal ionic conductivity and molecular stability. These findings identify guar gum as a promising, sustainable host polymer for sodium-based solid electrolytes in next-generation energy storage systems.

KEYWORDS: Polymeric materials; guar gum; sodium perchlorate; biopolymer electrolytes; ionic conductivity; X-ray diffraction analysis; density functional theory; HOMO–LUMO analysis

Copyright © 2026 The Authors. Published by Tech Science Press. This work is licensed under a Creative Commons Attribution 4.0 International License, which permits unrestricted use, distribution, and reproduction in any medium, provided the original work is properly cited.

1 Introduction

The United Nations' Sustainable Development Goal 7 highlights the importance of affordable, reliable, and sustainable energy access, underscoring the need for efficient energy storage systems. Sodium-based all-solid-state batteries have emerged as a promising alternative to lithium systems due to the natural abundance, low cost, and favourable electrochemical characteristics of sodium [1,2]. However, the performance of sodium-ion devices remains constrained by the properties of the BPEs. Traditional inorganic electrolytes suffer from interfacial instability and brittleness, motivating increasing interest in polymer and biopolymer electrolytes that offer improved flexibility, processability, and sustainability.

Natural biopolymers are particularly attractive because they are renewable, biodegradable, and environmentally benign [3,4]. Non-polysaccharide biopolymers such as poly(lactic acid) and polyhydroxyalkanoates often exhibit low ionic conductivity due to insufficient salt dissociation [5,6]. In contrast, polysaccharide-based materials such as alginate, cellulose derivatives, and chitosan provide oxygenated functional groups for ion coordination and hydrophilic networks that improve polymer segmental mobility [7,8]. Despite their versatility, the application of guar gum, a galactomannan polysaccharide widely used in industrial formulations, has been comparatively less investigated in sodium-ion conducting polymer electrolytes [9,10]. Although guar gum has received comparatively limited attention in solid polymer electrolyte systems, a previous study by Venkatesh et al. reported an ionic conductivity of 1.34×10^{-4} S cm^{-1} for a guar gum–based biopolymer electrolyte, indicating its strong potential for ion-conducting applications [11]. Thus, guar gum was selected as the host polymer due to its natural abundance, biodegradability, excellent film-forming ability, and high density of hydroxyl groups that can enhance ion–polymer interactions [12,13].

Next, $NaClO_4$ was selected as the added salt due to its high dissociation ability and strong interaction with polymer functional groups, which have been reported to enhance ionic conductivity, increase amorphous phase formation, and improve ion transport in polymer electrolyte systems [14]. $NaClO_4$ is also a suitable sodium salt for polymer electrolytes due to its bulky, weakly coordinating ClO_4^- anion, which enhances salt dissociation and disrupts polymer crystallinity, thereby improving Na^+ mobility [15,16]. Incorporating $NaClO_4$ into a guar gum matrix is therefore expected to increase amorphous character, provide more ion-conducting pathways, and enhance overall ionic transport. Accordingly, the variation in salt concentration was designed to investigate its influence on ionic conductivity and electrochemical properties systematically.

This study aims to develop guar gum–$NaClO_4$ biopolymer electrolytes and investigate how structural modifications influence their ion-transport behavior. EIS is employed to determine ionic conductivity and activation energy, while XRD is used to assess structural changes associated with salt loading. DFT calculations provide molecular-level insight into ion–polymer interactions and electronic stability. Together, these analyses establish a materials-level understanding of the guar gum–$NaClO_4$ system and its potential applicability as a sustainable biopolymer electrolyte for sodium-ion energy storage applications. Notably, this work establishes a direct structure–transport correlation by integrating XRD-derived amorphous character with impedance-derived ionic conductivity and DFT-based molecular insights into Na^+–polymer coordination, providing a multi-scale perspective on sodium-ion conduction in a guar gum-based biopolymer system that has been scarcely reported in previous biopolymer electrolyte studies.

2 Materials and Methods

2.1 Materials

Guar gum (Chemiz, Malaysia; food-grade; batch No. 2001191) was used as the host polymer. Sodium perchlorate ($NaClO_4$, ACS reagent grade, ≥98.0% purity, Sigma-Aldrich, USA; molecular weight 122.44 g·mol^{-1})

served as the sodium salt. Distilled water prepared using a double-distillation unit was used as the solvent throughout the study. All chemicals were used as received without further purification.

2.2 Preparation of Guar Gum–$NaClO_4$ Biopolymer Electrolytes

BPE films were prepared by solution casting. A total of 0.5 g of guar gum was used for each film, and $NaClO_4$ was incorporated at 0, 10, 20, 30, 40, and 50 wt.% relative to the polymer mass. Briefly, the appropriate mass of $NaClO_4$ was dissolved in 50 mL of distilled water in a clean glass bottle under continuous magnetic stirring until complete solubilization was achieved. Guar gum was then gradually introduced into the salt solution, followed by continuous stirring for 24 h at room temperature to obtain a homogeneous gel. The viscous gel was cast into Petri dishes and dried in an oven at 60°C for 24 h to ensure complete solvent evaporation. The dried films were carefully peeled off and stored in a desiccator at room temperature before characterization. Film thickness was measured at three random points using a digital micrometer, and the average value was used for conductivity calculations.

2.3 Electrochemical Impedance Spectroscopy

BPE Ionic conductivity measurements were performed at room temperature using a HIOKI 3532 LCR HiTester over the frequency range 100 Hz–1 MHz at an applied signal amplitude of 10 mV. Each BPE film was cut into circular discs and then sandwiched between two stainless-steel (SS) blocking electrodes under uniform pressure.

2.4 X-Ray Diffraction Analysis

Structural characterization was performed using a Bruker D8 Advance X-ray diffractometer operating at 40 kV and 30 mA with Cu Kα radiation (λ = 1.5406 Å). Scans were collected over $10^\circ \leq 2\theta \leq 80^\circ$ using a step size of 0.02° and a scan rate of $2^\circ \cdot min^{-1}$.

2.5 Density Functional Theory Methods

DFT calculations were performed using BIOVIA Materials Studio ($DMol^3$ module). Initial 2D structures of guar gum and $NaClO_4$ were constructed and converted to 3D atomistic models. Structures were pre-processed through hydrogen addition, valence validation, and geometry cleaning. All quantum chemical calculations were performed using the $DMol^3$ module. Geometry optimization was conducted using the Fine quality setting together with the hybrid B3LYP exchange–correlation functional. The Tkatchenko–Scheffler (TS) correction was applied to account for long-range dispersion interactions within the DFT-D framework. An unrestricted spin formalism was selected to allow independent treatment of the electronic spin channels in the calculations. Convergence limits were fixed at 1×10^{-5} Ha for the total energy, 0.002 Ha·Å^{-1} for the maximum force, and 0.005 Å for the maximum atomic displacement. The optimization procedure allowed 1000 Self-Consistent Field (SCF) iterations and used a maximum geometric step size of 0.3 Å. Electronic SCF cycles employed a tolerance of 1.0×10^{-6} Ha. The calculations evaluated the multipolar expansion of the charge density up to the hexadecapole level, employed charge density mixing with a mixing charge of 0.2 and a spin mixing value of 0.5, and used a density of states (DOS) basis set with a numerical size of 6 throughout the calculations, while applying electronic smearing of 0.005 Ha to assist SCF convergence.

Population analyses were carried out on the optimized structures. Mulliken population analysis was used to determine atomic charges, while Hirshfeld analysis was employed to quantify charge distribution and to examine charge transfer within the system.

3 Results and Discussions

3.1 Electrical Studies

An electrical characterization using electrochemical impedance spectroscopy (EIS) was performed to investigate the ionic conductivity of guar gum–$NaClO_4$ thin-film BPE with $NaClO_4$ contents ranging from 0 to 50 wt.% at room temperature. In this work, the 0 wt% composition refers to the guar gum biopolymer electrolyte without added salt, while all other samples contain $NaClO_4$ as the added salt. To further examine the effect of temperature, the samples with the lowest (0 wt.%) and highest (40 wt.%) ionic conductivities were subjected to temperature-dependent EIS measurements from 300 K to the maximum ionic conductivity.

3.1.1 Room-Temperature Ionic Conductivity

Fig. 1 shows the impedance plots (Z_i vs. Z_r) for all prepared samples at room temperature (300 K). The 0 wt.% sample exhibits a semicircle, while the other compositions display a straight line. The observed semicircles in the complex plane are often distorted and enlarged, producing asymmetric arcs with their centers positioned below the real Z_r axis. The semicircle diameter corresponds to the charge-transfer resistance, with a larger diameter indicating higher resistance [17,18]. Accordingly, the 0 wt.% sample exhibited the largest semicircle diameter, indicating greater charge-transfer resistance than the $NaClO_4$-added samples with 10, 20, 30, 40, and 50 wt.% salt content.

The negative imaginary component (Z_i) plotted against the real component (Z_r) provides the bulk resistance (R_b) from the intercept at Z_r [19]. The high-frequency semicircle corresponds to bulk resistance, while the low-frequency spike arises from double-layer charge accumulation at the BPE|electrode interface [20]. The ionic conductivity (σ) was calculated using Eq. (1):

$$\sigma = \frac{t}{R_b A} \tag{1}$$

where t is the film thickness, A is the electrode contact area, and R_b is the bulk resistance obtained from the high-frequency intercept of the impedance plot.

The composition-dependent ionic conductivity is influenced by both charge carrier concentration and mobility [21]. Accordingly, the 40 wt% $NaClO_4$ sample exhibits the highest ionic conductivity, which is associated with the lowest R_b, as summarized in Table 1. Table 1 summarizes the impedance-derived bulk resistance (R_b), corresponding electrical conductance (G), and calculated ionic conductivity (σ) of guar gum–$NaClO_4$ biopolymer electrolytes, clearly demonstrating a progressive decrease in R_b and a corresponding increase in G and σ with increasing $NaClO_4$ content up to the optimum composition, followed by a decline at higher salt loading.

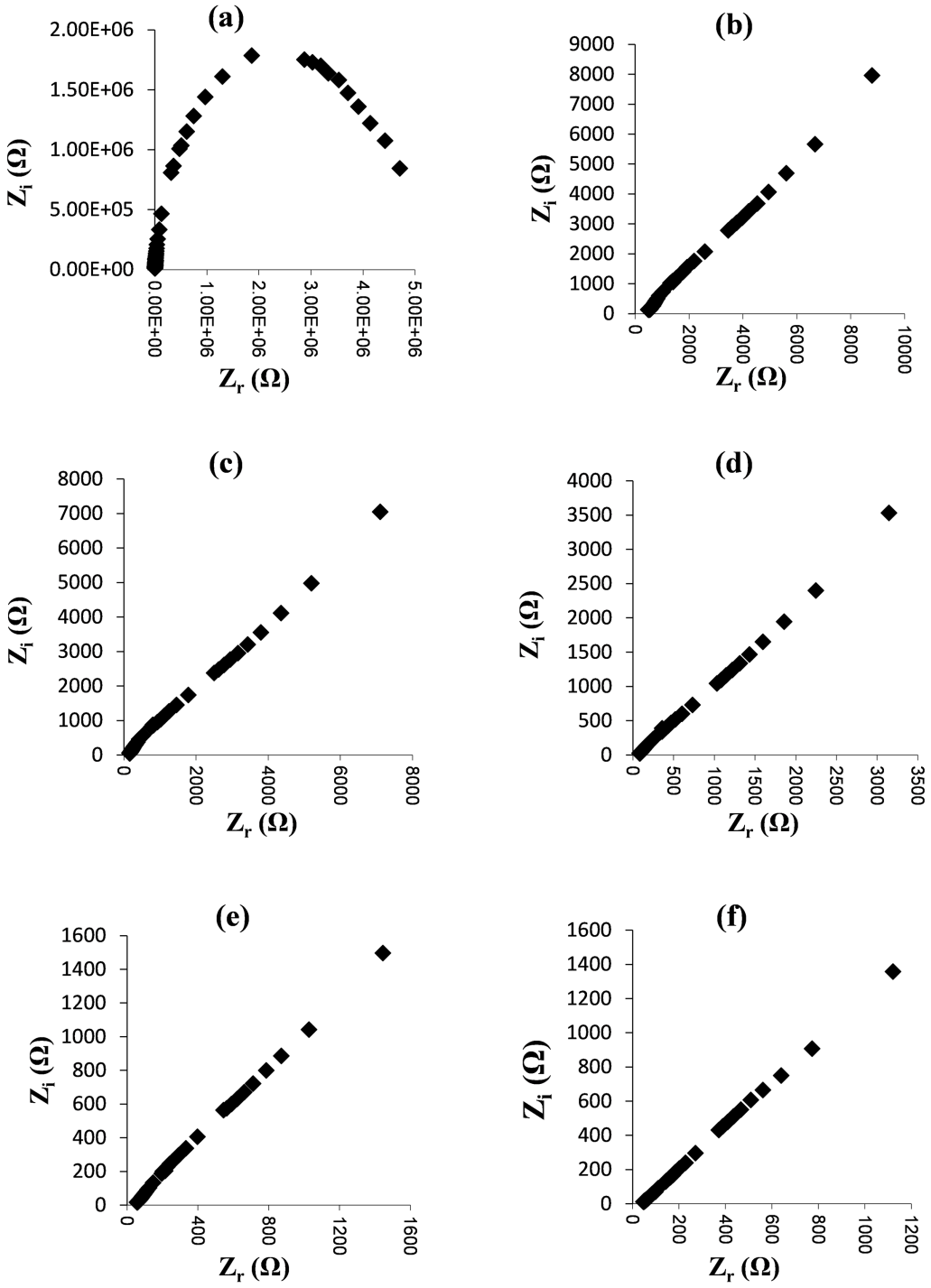

Figure 1: Nyquist plots of guar gum–$NaClO_4$ biopolymer electrolytes at different salt concentrations: (**a**) 0 wt%, (**b**) 10 wt%, (**c**) 20 wt%, (**d**) 30 wt%, (**e**) 40 wt%, and (**f**) 50 wt% $NaClO_4$.

Table 1: Impedance-derived bulk resistance, conductance, and corresponding ionic conductivity values for guar gum-based biopolymer electrolytes with varying $NaClO_4$ loadings.

Sample (wt.%)	Bulk Resistance, R_b (Ω)	Conductance, G (S)	Ionic Conductivity, σ ($S{\cdot}cm^{-1}$)
0	5,020,000.0	1.99×10^{-7}	4.45×10^{-9}
10	4120.0	2.43×10^{-4}	5.43×10^{-6}
20	315.0	3.17×10^{-3}	7.09×10^{-5}
30	53.5	1.87×10^{-2}	4.18×10^{-4}
40	26.6	3.76×10^{-2}	8.40×10^{-4}
50	66.3	1.51×10^{-2}	3.37×10^{-4}

Based on Fig. 2, ionic conductivity increases progressively with $NaClO_4$ salt content, from 9.13×10^{-9} $S{\cdot}cm^{-1}$ for the unadded $NaClO_4$ salt sample (0 wt.%) to 6.31×10^{-4} $S{\cdot}cm^{-1}$ at 50 wt.% $NaClO_4$, reflecting enhanced $NaClO_4$ ion dissociation and mobility [19]. However, the maximum ionic conductivity of 8.40×10^{-4} $S{\cdot}cm^{-1}$ is obtained at 40 wt.% $NaClO_4$. Beyond this concentration, ionic conductivity decreases due to ion–ion pairing, ionic cross-linking, and increased viscosity, which limit free ion mobility [22].

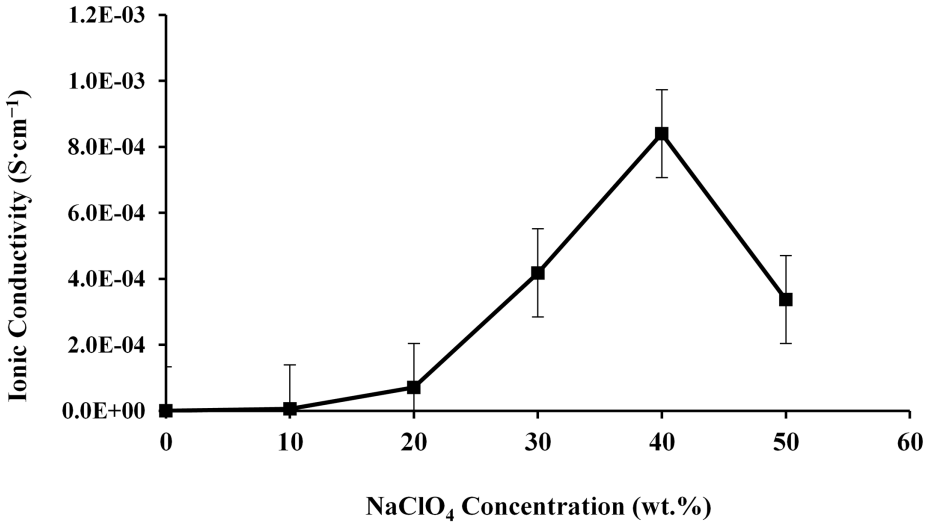

Figure 2: Salt concentration–dependent ionic conductivity behavior of guar gum–$NaClO_4$ biopolymer electrolytes.

The ionic conductivity achieved in the present guar gum–based polymer electrolyte is comparable to or higher than several previously reported biopolymer electrolyte systems, such as corn starch-based, chitosan-based, and cellulose-based electrolytes, which exhibit maximum ionic conductivities of 1.28×10^{-4} $S{\cdot}cm^{-1}$ [23], 7.34×10^{-5} $S{\cdot}cm^{-1}$ [24], 2.53×10^{-4} $S{\cdot}cm^{-1}$ [25], respectively. Compared with these systems, guar gum offers a highly flexible polymer backbone with abundant hydroxyl functional groups, which promote strong coordination with sodium ions and facilitate efficient ion transport [26,27].

To further clarify the correlation between impedance response and ionic conductivity, the bulk resistance (R_b) obtained from the high-frequency intercept was expressed in terms of electrical conductance [28,29]:

$$G = \frac{1}{R_b} \tag{2}$$

Substituting this relationship into the conductivity expression yields an equivalent form [28,29]:

$$\sigma = \frac{L}{A} \times G \tag{3}$$

where L is the membrane thickness and A is the effective electrode–electrolyte contact area. This formulation shows directly that ionic conductivity is proportional to conductance for a given sample geometry. Therefore, the observed increase in G with $NaClO_4$ loading corresponds to a reduction in R_b and translates into a higher σ, explaining why the highest-conductivity composition also exhibits the highest conductance.

3.1.2 Temperature-Dependent Ionic Conductivity

The sample with 40 wt.% $NaClO_4$, which exhibited the highest ionic conductivity at room temperature, was selected for further investigation. Impedance measurements were performed at 303, 313, 323, 333, and 343 K for samples containing 0, 30, and 40 wt.% $NaClO_4$. Measurements at 353 K were also attempted. However, non-reproducible impedance responses were observed, likely due to partial dehydration of the BPE films. Therefore, the temperature-dependent analysis was limited to the 303–343 K range to ensure data reliability. The temperature-dependent analysis enabled the determination of the activation energy (E_a) of ionic conduction, a key parameter for optimizing electrolyte performance [30]. The relationship between ionic conductivity and temperature follows the Arrhenius equation:

$$\sigma = \sigma_0 \, exp\left(\frac{-E_a}{k_B T}\right) \tag{4}$$

where σ_0 is the pre-exponential factor, k_B is the Boltzmann constant, and T is the absolute temperature. Plotting log (ionic conductivity) against 1000/T produced a linear relationship (Fig. 3A), confirming that the guar gum biopolymer electrolyte films obey the Arrhenius model with regression values close to unity ($R^2 \approx 1$) [31]. Such behavior indicates that ionic conduction occurs predominantly via thermally activated hopping of Na^+ ions between localized sites, analogous to the mechanism in ionic crystals [30].

As temperature increases, both the mobility and dissociation rate of Na^+ ions rise, enhancing ionic conductivity. This improvement is attributed to increased free volume and segmental motion in the guar gum biopolymer matrix, which facilitate Na^+ ion transport. The observed decrease in activation energy with increasing ionic conductivity (Fig. 3B) supports this mechanism. Specifically, the 40 wt.% $NaClO_4$ sample demonstrated the lowest activation energy (7.61×10^{-20} eV), corresponding to its highest ionic conductivity. Lower activation energy reduces the energy barrier to Na^+ ion migration, thereby enhancing charge-carrier mobility and overall ionic conductivity.

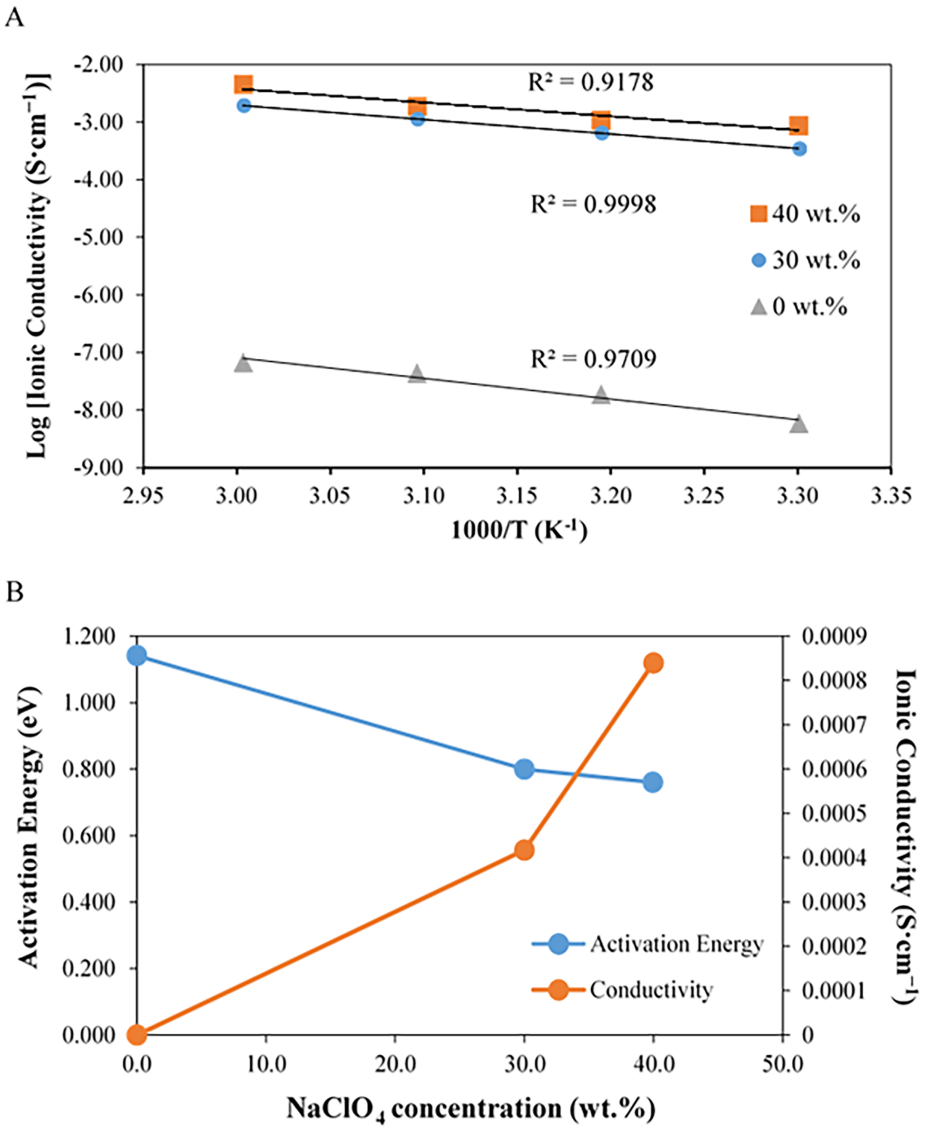

Figure 3: Temperature-dependent ionic conductivity and activation energy of BPEs with varying $NaClO_4$ concentrations. (**A**) Arrhenius plots of log (ionic conductivity) vs. 1000/T for BPEs containing 0, 30, and 40 wt.% $NaClO_4$, showing linearity consistent with thermally activated ion transport. (**B**) Variation of activation energy and room-temperature ionic conductivity as functions of $NaClO_4$ concentration.

3.1.3 Dielectric Studies

Dielectric studies are essential for interpreting the ionic conductivity behavior of guar gum–$NaClO_4$ BPE, as they reveal the coupling between ion transport processes and the relaxation dynamics of guar gum biopolymer chains. The complex permittivity (ε^*) of an electrolyte is strongly influenced by its structural characteristics, temperature, and applied field frequency [32]. In this work, the sample containing 40 wt.% $NaClO_4$, which exhibited the highest ionic conductivity, was selected as a representative composition for detailed dielectric evaluation. The dielectric constant (ε_r) and dielectric loss (ε_i) of this system are analyzed to elucidate the relationship between ion transport, polymer segmental dynamics, and polarization mechanisms. The variations in ε_r and ε_i as a function of frequency are depicted in Fig. 4A,B.

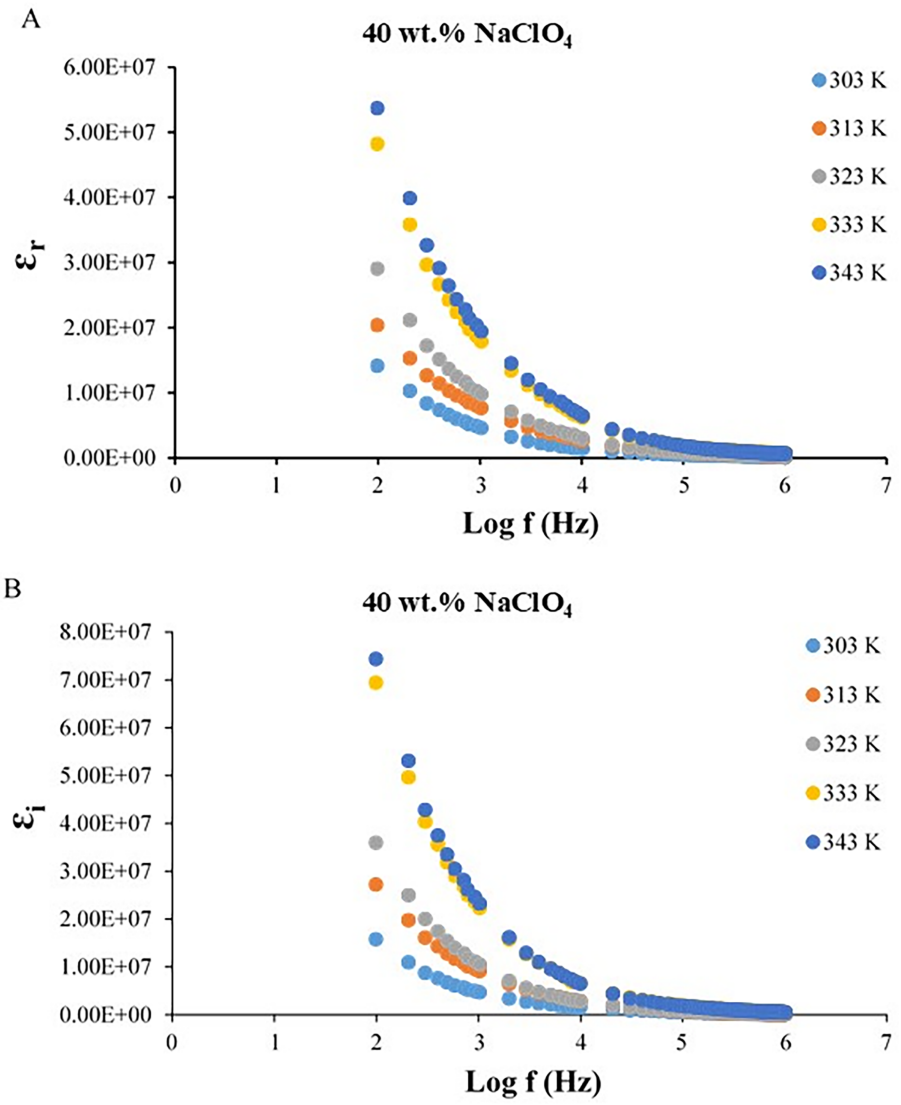

Figure 4: Temperature influence on the dielectric behavior of the guar gum-based biopolymer electrolyte incorporated with 40 wt.% $NaClO_4$. (**A**) Plot of dielectric constant (ε_r) vs. logarithmic frequency at different temperatures. (**B**) Plot of dielectric loss (ε_i) vs. logarithmic frequency at different temperatures. Abbreviations: ε_r = dielectric constant; ε_i = dielectric loss.

The dielectric constant (ε_r) represents the material's ability to store charge, while the dielectric loss (ε_i) corresponds to the energy dissipated due to ion migration under an alternating electric field. At low frequencies, both ε_r and ε_i exhibit sharp increases, attributed to electrode polarization and space-charge accumulation, confirming the non-Debye relaxation behavior of the system. At higher frequencies, the rapid reversals of the electric field hinder ion displacement, leading to a decline in ε_r and ε_i as polarization becomes less effective [32]. At low frequencies, the dielectric loss ε_i values exceeded ε_r, indicating significant ionic conduction and interfacial polarization in the guar gum–$NaClO_4$ system. This behavior suggests enhanced mobility of dissociated Na^+ ions, consistent with increased dissociation of $NaClO_4$. The dielectric loss response is mainly governed by the combined effects of DC conductivity and polarization processes [19].

Fig. 5A,B presents the frequency dependence of the real (M_r) and imaginary (M_i) components of the electric modulus, measured over a temperature range of 303–343 K. As observed, both M_r and M_i approach zero at low frequencies, indicating the dominance of electrode polarization and the presence of long-range ionic motion. With increasing frequency, the modulus values rise, with M_r consistently exceeding M_i, signifying the onset of bulk relaxation processes within the guar gum biopolymer electrolyte matrix. A noticeable decrease in the magnitudes of both M_r and M_i with increasing temperature suggests enhanced ionic mobility, as thermal activation promotes faster ion migration and the segmental motion of the guar gum biopolymer [33–36]. Among the investigated compositions, the electrolyte with the highest $NaClO_4$ concentration exhibited the highest modulus values, indicating that $NaClO_4$ salt incorporation influences ionic relaxation strength and charge-carrier density [37–39].

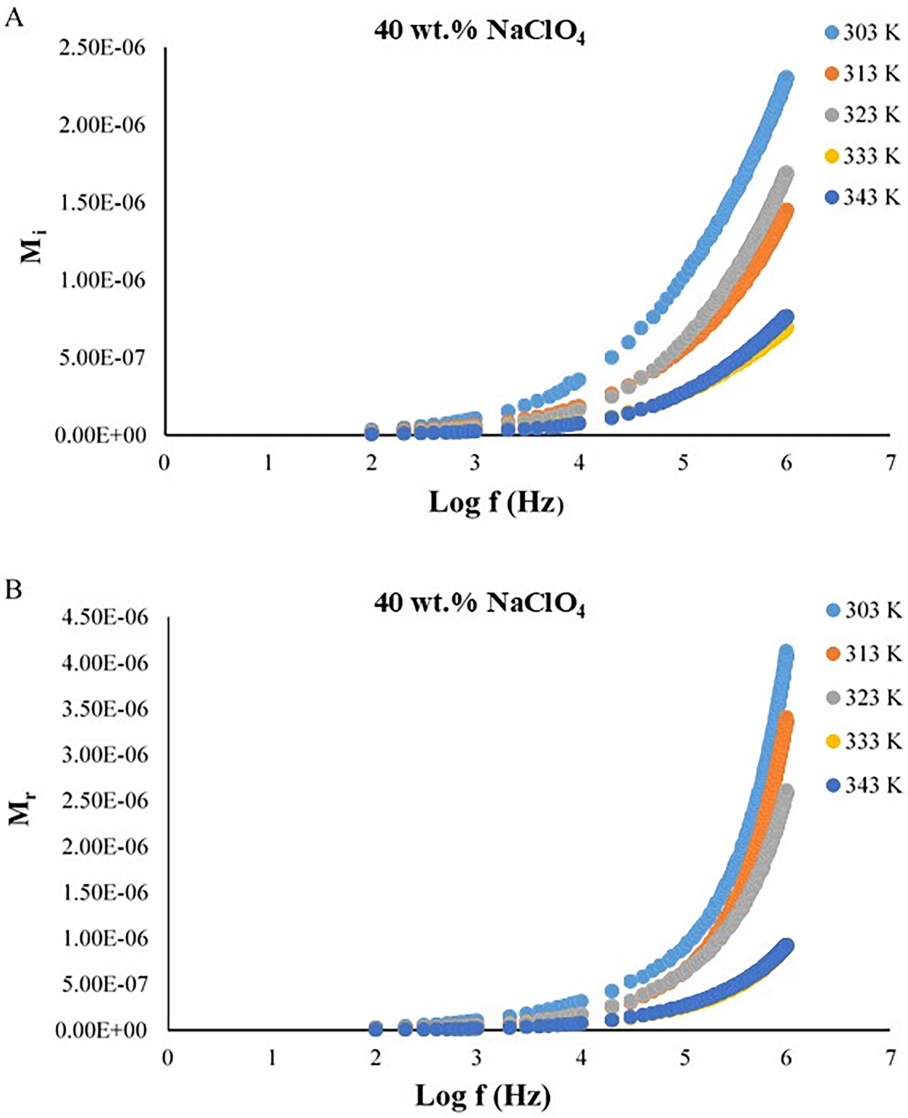

Figure 5: Temperature influence on the electrical modulus of the guar gum-based biopolymer electrolyte incorporated with 40 wt.% $NaClO_4$. (**A**) Imaginary modulus (M_i) as a function of logarithmic frequency at different temperatures. (**B**) Real modulus (M_r) as a function of logarithmic frequency at different temperatures. Abbreviations: M_i = imaginary modulus; M_r = real modulus.

The M_r spectra, which remain nearly zero at low frequencies and peak at higher frequencies, further confirm the suppression of electrode polarization and the predominance of bulk relaxation phenomena in the high-frequency region. These frequency-dependent trends reflect the ion dynamics within the guar gum biopolymer matrix. At low frequencies, ions can align effectively with the alternating electric field, yielding smaller modulus values. However, as frequency increases, the ions are unable to follow the rapidly oscillating field, leading to an increase in modulus magnitude [33,40–42]. The overall decline in modulus with temperature reinforces the concept of thermally activated ionic transport, consistent with the observed enhancement in ionic conductivity at elevated temperatures.

3.2 Structural Studies

Structural study by XRD reveals the effect of $NaClO_4$ loading on the crystalline–amorphous structure of guar gum electrolyte films. As shown in Fig. 6 and Table 2, XRD analysis shows progressive broadening of the major diffraction halo with increasing $NaClO_4$ concentration, reflecting a loss of long-range chain order and a greater fraction of amorphous domains. The XRD patterns of the 0 wt.% and 10 wt.% $NaClO_4$ samples are dominated by a broad amorphous halo, consistent with the predominantly amorphous nature of biopolymer electrolyte films reported in recent literature, where XRD profiles exhibit a broad amorphous background that increases with salt content and reflects limited long-range ordering. Such features have been similarly interpreted in XRD studies of biopolymer electrolytes, where broadening of diffraction maxima corresponds to increased amorphous character rather than well-defined crystalline phases [43,44]. Crystallite size was estimated using the Scherrer equation, employing the full width at half maximum (FWHM) of the dominant diffraction peak.

$$D = \frac{K\lambda}{\beta \cos\theta} \tag{5}$$

where D represents the average crystallite size (nm), K is the shape factor (commonly taken as 0.9), λ is the wavelength of the incident X-ray beam (Cu Kα, λ = 1.5406 Å), β denotes the full width at half maximum (FWHM) of the diffraction peak, and θ is the corresponding Bragg diffraction angle. The dominant diffraction peak for each composition was selected from the deconvoluted XRD profiles, and the corresponding FWHM values were used for crystallite size calculation after instrumental broadening correction.

This structural change is quantitatively detected by a sharp diminution in Scherrer crystallite size from 5.05 nm at 0 wt.% to 0.82 nm at 40 wt.%, $NaClO_4$. The increase in amorphous character enhances segmental mobility within the guar gum matrix, facilitating the flow of Na ions through guar gum biopolymer coordination sites. Room-temperature ionic conductivity therefore increases very significantly from 9.13×10^{-9} S·cm^{-1} (0 wt.%) to 8.40×10^{-4} S·cm^{-1} (40 wt.%). This strong structure–transport correlation aligns with previous findings in polymer–salt systems, where salt-induced amorphization significantly lowers the energy barrier to Na^+ ion hopping and enhances overall ionic mobility within the polymer matrix [7,45,46]. A guar gum biopolymer electrolyte with a higher amorphous content exhibits greater segmental mobility and backbone flexibility. This segmental mobility facilitates ionic transport under an electric field by continuously forming and breaking the coordination spheres of solvated ions. Consequently, more free volume becomes available for ion diffusion [19].

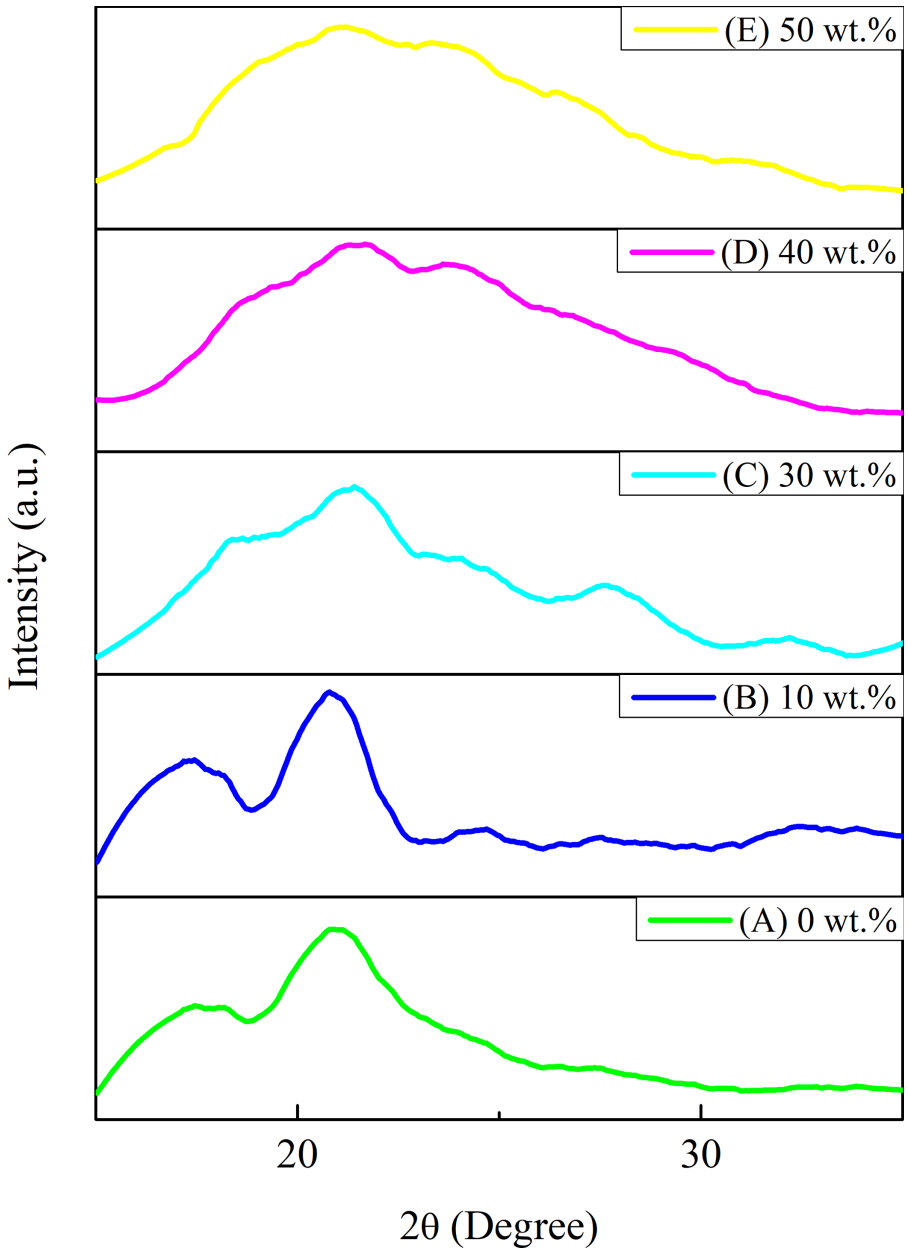

Figure 6: XRD patterns of guar gum–$NaClO_4$ biopolymer electrolytes (BPEs) with increasing salt content. Sample containing (**A**) 0 wt.% $NaClO_4$. (**B**) 10 wt.% $NaClO_4$. (**C**) 30 wt.% $NaClO_4$. (**D**) 40 wt.% $NaClO_4$. (**E**) 50 wt.% $NaClO_4$. Abbreviations: XRD = X-ray diffraction; BPE = biopolymer electrolyte.

Table 2: Crystallite size and corresponding room-temperature ionic conductivity for guar gum samples at various $NaClO_4$ loadings.

Salt Concentration (wt.%)	2θ (°)	FWHM (°)	Crystallite Size (nm)	Ionic Conductivity, σ ($S{\cdot}cm^{-1}$)
0	20.70	1.59992	5.0488	9.13×10^{-9}
10	21.09	6.83702	1.1817	5.43×10^{-5}
40	22.82	9.87954	0.8179	8.40×10^{-4}
50	22.38	8.84732	0.9161	3.37×10^{-4}

3.3 Electronic Studies

DFT is employed to elucidate electronic interactions and charge-transfer behavior within the biopolymer electrolyte system. The primary aim of this study is to correlate the electronic structure with the observed ionic conductivity, thereby providing a molecular-level understanding of ion coordination and mobility. DFT calculations yield the optimized molecular geometry, HOMO–LUMO energy band gap, and density of states (DOS), which reflect the energy distribution and electronic stability of the system. In addition, Raman spectral analysis derived from DFT helps validate vibrational modes associated with guar gum–$NaClO_4$ complexation. Collectively, these electronic descriptors establish the fundamental relationship between the molecular configuration and the electrochemical performance of the electrolyte.

3.3.1 Optimized Molecular Structure of the Biopolymer Guar Gum

Guar gum is a natural, non-ionic polysaccharide composed of a polymannose chain containing (1 → 4)-linked β-D-mannopyranose units and α-D-galactopyranose side groups attached through (1 → 6) glycosidic linkages to the mannose backbone. The mannose-to-galactose ratio typically ranges from 1.8 to 1.0 [47]. According to Jain et al. [47], a representative structural model of guar gum consists of two (1 → 4)-linked mannose units, with a galactose branch attached to one of the mannose units via a (1 → 6) linkage. In the present study, a sodium perchlorate ($NaClO_4$) molecule was incorporated into the guar gum model to investigate the molecular interactions between the guar gum biopolymer matrix and the $NaClO_4$ salt. Fig. 7A presents the molecular structure before optimization, while Fig. 7B shows the optimized guar gum–$NaClO_4$ complex with evident Na^+ migration and ClO_4^- reorientation. The optimized guar gum–$NaClO_4$ complex contains 70 atoms and includes five elements: carbon (C), hydrogen (H), oxygen (O), sodium (Na), and chlorine (Cl).

The objective of geometry optimization in DFT is to determine the lowest possible ground-state energy while simultaneously achieving the most stable molecular configuration through atomic repositioning [48]. The geometry optimization led to a gradual decrease and stabilization of the total energy at −2980.03 Ha, confirming that the system achieved full convergence and reached its minimum-energy configuration (Fig. 8A). These optimized structural parameters ensured a stable equilibrium suitable for subsequent electronic structure analysis.

The convergence profile illustrated in Fig. 8B shows the logarithmic ($\log_{10}$) variation of the energy change (black), maximum displacement (red), and maximum force (blue) with successive optimization steps. All three parameters exhibit a steady decrease over the initial ~10–15 steps, indicating efficient structural relaxation, and subsequently approach asymptotic values, confirming stable convergence. A recent DFT study by Boshoman and Fatoba [48] reported similar convergence behavior, supporting the reliability of the present optimization results.

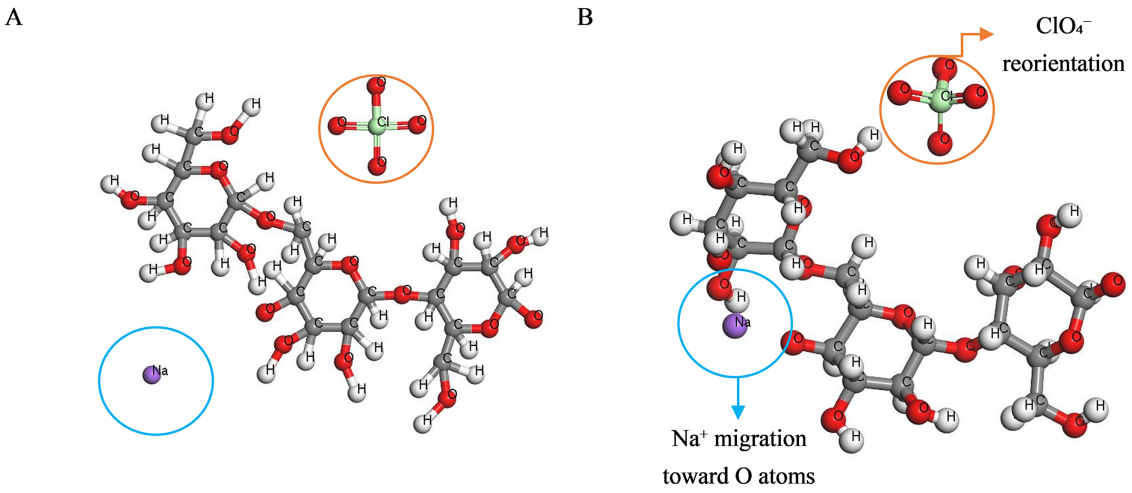

Figure 7: Three-dimensional molecular structures of the guar gum–$NaClO_4$ complex. (**A**) Structure before geometry optimization. (**B**) Structure after geometry optimization, showing Na^+ migration toward O atoms and ClO_4^- reorientation. Abbreviations: C = carbon; H = hydrogen; O = oxygen; Na = sodium; Cl = chlorine.

The DMol^3 geometry optimization of the guar gum–$NaClO_4$ adduct shows a rapid initial energy drop followed by a smooth approach to a stationary point, with forces and displacements decreasing monotonically. This behavior is characteristic of a well-converged Kohn–Sham DFT minimum [49]. The convergence indicates the formation of a mechanically stable coordination complex, where Na^+ ions are solvated by hydroxyl and ether oxygens from the polysaccharide backbone. This coordination motif has been widely reported for cation binding in guar gum biopolymer electrolytes [50,51]. As shown in Fig. 8B, DMol^3 geometry optimization drove the guar gum–sodium perchlorate complex to its lowest-energy configuration by effectively minimizing the atomic forces to achieve equilibrium.

3.3.2 Density of States Analysis

The density of states (DOS) represents the distribution of available electronic states across different energy levels. It serves as a key indicator of the charge transport and electronic behavior of materials. In solid-state and condensed-matter systems, the DOS determines how electrons occupy energy bands and directly influences a material's electronic conduction properties. As reported by Mostefai [52], the total DOS can be evaluated by projecting the electron density of each atom onto spherical harmonics (s, p, d, or f orbitals), allowing identification of orbital contributions to bonding interactions. Variations in the DOS can indicate changes in band and Fermi energies, which, in turn, affect electronic conductivity and other electronic properties [53]. Furthermore, recent studies have demonstrated that machine learning models can leverage DOS data to efficiently predict material properties, thereby improving the accuracy of electronic-structure predictions [53,54].

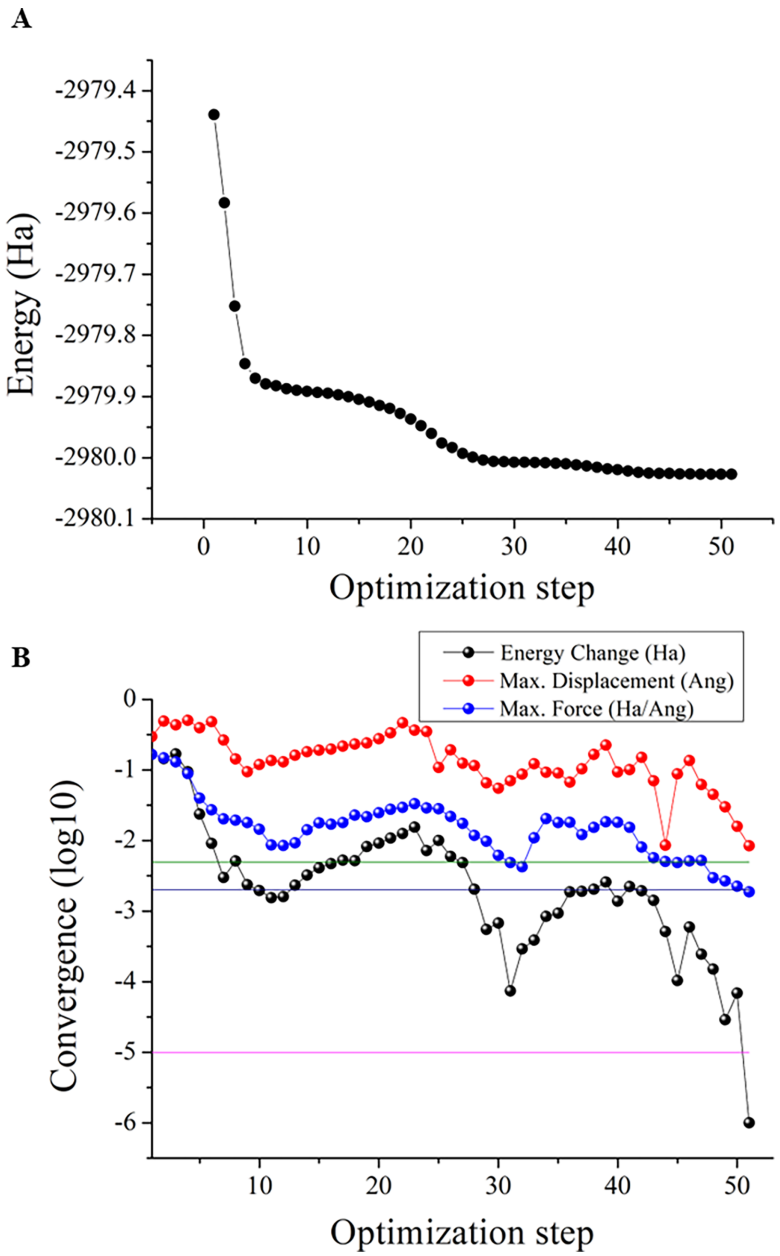

Figure 8: Geometry optimization behavior of the guar gum–$NaClO_4$ complex. (**A**) Energy variation plotted against optimization steps. (**B**) Convergence profiles during optimization, showing energy change, maximum displacement, and maximum force. Abbreviations: Ha = Hartree (energy unit).

In the guar gum–$NaClO_4$ biopolymer electrolyte, DOS analysis provides valuable insight into how $NaClO_4$ salt incorporation modifies the electronic structure, promotes orbital interactions, and enhances charge transport within the guar gum biopolymer matrix. Fig. 9A presents the total density of states (DOS) of the guar gum–$NaClO_4$ complex, plotted as a function of energy in electron-volts (eV), while Fig. 9B shows the corresponding DOS plotted in Hartree (Ha) units, illustrating the distribution of electronic states and the contribution of occupied valence levels near the Fermi energy. The DOS vs. energy plot shows multiple broad peaks between –600 eV and 0 eV (or –20 Ha to 0 Ha), corresponding to the valence orbitals of oxygen

and carbon from guar gum, as well as oxygen and chlorine orbitals from $NaClO_4$. A pronounced shift in the DOS toward the Fermi level is observed following complexation, suggesting electronic coupling and donor–acceptor interactions between guar gum oxygen sites and Na^+ ions from the $NaClO_4$ salt. Signals near the Fermi level (E = 0 eV) represent DOS features approaching the Fermi edge, thus their convergence indicates reduced HOMO–LUMO separation and increased electronic polarizability that enhances dielectric screening and facilitates the dissociation of $NaClO_4$ into free Na^+ and ClO_4^- ions, while actual ionic conductivity remains governed by Na^+ coordination dynamics and guar gum biopolymer segmental motion.

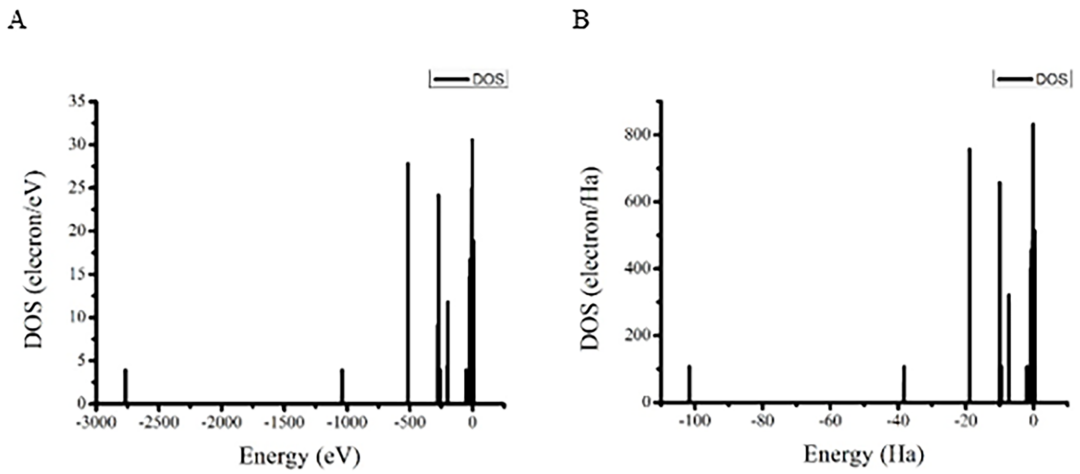

Figure 9: Total density of states (DOS) of the guar gum–$NaClO_4$ complex plotted as a function of energy in (**A**) electronvolt (eV) and (**B**) Hartree (Ha) units, illustrating the distribution of electronic states and the contribution of occupied valence levels near the Fermi energy.

This shift in the DOS indicates an increased density of accessible electronic states near the Fermi level, suggesting enhanced electronic delocalization and a greater propensity for charge-transfer within the guar gum–$NaClO_4$ matrix. The slight separation between the valence and conduction regions implies moderate electronic conductivity, which supports the material's suitability for solid-state electrolyte applications.

3.3.3 The Frontier Molecular Orbitals Analysis

The frontier molecular orbitals (FMOs), including the highest occupied molecular orbital (HOMO) and the lowest unoccupied molecular orbital (LUMO), are crucial for understanding charge-transfer interactions in polymer electrolyte systems [55]. The HOMO represents the electron-donating capacity, while the LUMO indicates the electron-accepting ability of the molecule [2]. The HOMO–LUMO energy band gap reflects the compound's chemical reactivity and kinetic stability. A smaller band gap generally indicates enhanced charge-transfer capability and increased molecular softness, which are favorable for promoting salt dissociation and interfacial polarization in polymer electrolyte materials. In this study, the HOMO–LUMO energy band gap of the BPE system was analyzed to assess its electronic stability and potential contribution to electrochemical performance. The corresponding molecular orbital distributions and energy levels are illustrated in Fig. 10.

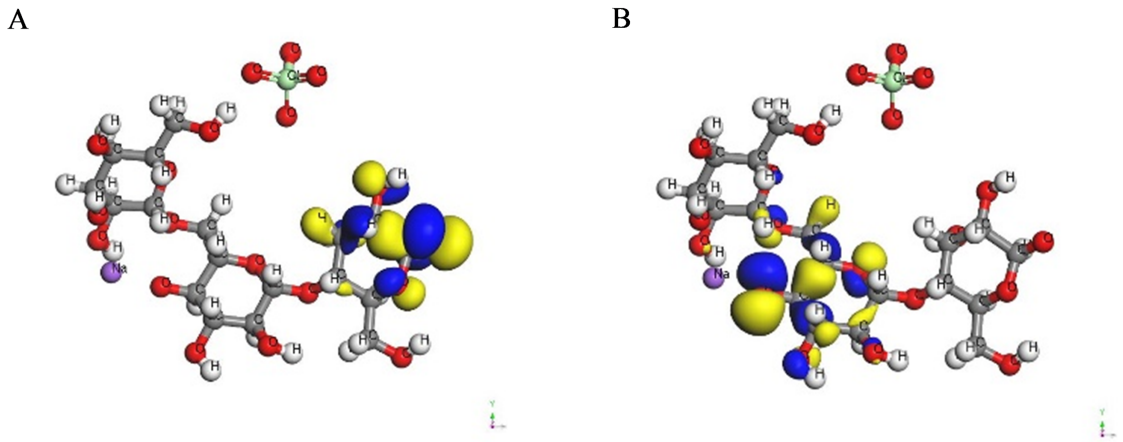

Figure 10: Frontier molecular orbital distributions of the guar gum–$NaClO_4$ system. (**A**) Highest occupied molecular orbital (HOMO) distribution. (**B**) Lowest unoccupied molecular orbital (LUMO) distribution. Abbreviations: HOMO = highest occupied molecular orbital; LUMO = lowest unoccupied molecular orbital.

As illustrated in Fig. 10A, the highest occupied molecular orbital (HOMO) distribution of the guar gum–$NaClO_4$ system is shown, while Fig. 10B presents the lowest unoccupied molecular orbital (LUMO) distribution, illustrating the spatial characteristics of the frontier molecular orbitals. The blue region corresponds to the negative phase, while the yellow region represents the positive phase of the molecular orbitals. The energy band gap (ΔE) and several quantum-chemical parameters of the unadded guar gum sample were obtained from the study by Kazachenko et al. [55]. In contrast, the energy band gap of the guar gum–$NaClO_4$ system was calculated using the relation:

$$\Delta E = E_{LUMO} - E_{HOMO} \tag{6}$$

The calculated results reveal that the guar gum–$NaClO_4$ complex exhibits a substantially reduced energy band gap of 0.3813 eV, compared to 6.6129 eV for unadded salt guar gum, indicating enhanced electronic polarizability and improved charge-transfer interactions within the polymer–salt complex. This reduction in band gap is attributed to the coordination between Na^+ ions and the oxygen-containing functional groups of guar gum, which modifies the electronic structure and facilitates donor–acceptor interactions. Such electronic flexibility supports salt dissociation and interfacial polarization, while ionic conductivity remains primarily governed by Na^+ transport and polymer segmental motion. To further evaluate the chemical reactivity of the guar gum–$NaClO_4$ system, several quantum-chemical parameters were derived from the HOMO and LUMO energy values and summarized in Table 3. The parameter values for the unadded salt guar gum sample were obtained from Kazachenko et al. [55], and the corresponding parameters for the guar gum–$NaClO_4$ system were calculated using the equations reported in the same study:

$$I = -E_{HOMO} \tag{7}$$

$$A = -E_{LUMO} \tag{8}$$

$$\chi = \frac{(I + A)}{2} \tag{9}$$

$$\eta = \frac{(I - A)}{2} \tag{10}$$

$$\mu = -\chi \tag{11}$$

$$\Delta N_{max} = \frac{-\mu}{\eta} \quad (12)$$

$$\varsigma = \frac{1}{\eta} \quad (13)$$

$$\omega = \frac{\mu^2}{2\eta} \quad (14)$$

The guar gum–$NaClO_4$ system exhibits low chemical hardness (0.1907 eV) and high softness (5.2440 eV^{-1}), reflecting enhanced electronic flexibility and polarizability. In addition, the system exhibits the largest ΔN_{max} (33.3769), suggesting superior charge-exchange capacity between donor and acceptor orbitals. These features favor strong polymer–salt interactions and enhance electrochemical performance while maintaining the ionic nature required for solid-state electrolyte applications.

Table 3: Selected electronic properties of unadded salt Guar gum and Guar gum–$NaClO_4$ systems.

Parameters	Unadded Salt Guar Gum	Guar Gum–$NaClO_4$
E_{HOMO} (eV)	−7.0262	−6.5539
E_{LUMO} (eV)	−0.4133	−6.1726
Energy band gap (ΔE) (eV)	6.6129	0.3813
Chemical Potential (μ) (eV)	−3.7197	−6.3633
Softness (ς) (eV^{-1})	0.3024	5.2440
Ionization energy (I) (eV)	7.0262	6.5539

4 Conclusions

This study confirms that guar gum is a viable polymer host for biopolymer electrolytes, achieving the highest ionic conductivity of 8.40×10^{-4} S cm^{-1} at 40 wt.% $NaClO_4$. Conductivity increased with salt concentration up to this optimum due to enhanced free-ion mobility, but declined at higher loadings because of ion–ion pairing, ionic cross-linking, and viscosity effects. Dielectric analysis of the optimum sample showed electrode polarization at low frequencies and characteristic decay at high frequencies, while modulus behaviour supported long-range ion mobility. Temperature-dependent results further indicated thermally assisted dipole and ion motion. XRD patterns confirmed a decrease in crystallinity and an increase in amorphousness with salt addition, with the smallest crystallite size (0.8179 nm) corresponding to the highest-conductivity sample. Collectively, while the present work focuses on structural, dielectric, and ion-transport characterization, device-level electrochemical performance evaluation (e.g., CV and LSV in full cells) is beyond the scope of this study. Nevertheless, the optimized guar gum–$NaClO_4$ electrolyte exhibits high room-temperature ionic conductivity and favorable polarization and relaxation behavior, which are key prerequisites for solid-state electrolyte materials intended for energy storage systems. Future work will include electrochemical stability and full device testing to further validate its practical applicability. DFT analysis provided molecular-level insight into the coordination and charge-transfer mechanisms within the guar gum–$NaClO_4$ biopolymer electrolyte. Geometry optimization confirmed the formation of a stable guar gum–$NaClO_4$ complex, where Na^+ interacts strongly with hydroxyl and ether oxygen sites of the polysaccharide backbone. DOS analysis revealed enhanced electronic coupling and a shift of electronic states toward the Fermi level, indicating increased electronic polarizability that supports salt dissociation within the matrix. Frontier molecular orbital analysis further showed a substantial reduction in the HOMO–LUMO energy gap (0.3813 eV), demonstrating improved charge-transfer capability and greater electronic flexibility

compared to unadded salt guar gum sample. Together, these computational descriptors establish a clear link between molecular configuration, electronic structure, and the enhanced ion-coordination environment responsible for the improved electrochemical performance of the guar gum–$NaClO_4$ electrolyte.

Acknowledgement: The authors would like to thank the iMADE Research Laboratory, Institute of Science, Faculty of Applied Sciences, Universiti Teknologi MARA (UiTM) for providing research facilities for this project.

Funding Statement: The authors received no specific funding for this study.

Author Contributions: All authors contributed substantially according to the journal's authorship criteria. Siti Zafirah Zainal Abidin conceptualised the research idea, supervised the experimental design, and contributed to data interpretation. Rabiatul Akashah Rusli carried out the sample preparation and characterizations (electrical and structural). Nur Farisha Sulthan Hussain performed the density functional theory (DFT) calculations (electronic). Siti Rudhziah Che Balian supported data analysis, validation, and technical revisions. All authors contributed to the drafting or critical revision of the manuscript, approved the final version, and agree to be accountable for all aspects of the work. All authors reviewed and approved the final version of the manuscript.

Availability of Data and Materials: The data and code that support the findings of this study are available from the corresponding author upon reasonable request.

Ethics Approval: Not applicable.

Conflicts of Interest: The authors declare no conflicts of interest.

References

1. Oh JAS, Yu Z, Huang CJ, Ridley P, Liu A, Zhang T, et al. Metastable sodium closo-hydridoborates for all-solid-state batteries with thick cathodes. Joule. 2025;9(10):102130. doi:10.1016/j.joule.2025.102130.
2. Gupta P, Gupta AK, Gupta SK, Gupta S, Shriwastav M, Yadav RK. DFT study on Na-ion conducting solid biopolymer electrolyte-based on agar-agar and $NaPF_6$ for sodium-ion batteries. Nano Hybrids Compos. 2023;40:65–78. doi:10.4028/p-rz9jfl.
3. Selvi TM, Brindha S, Kumar PM, Mareeswaran V, Muthuraaman B, Suthanthiraraj SA. Bio-based polymer electrolytes for electrochemical applications—an overview. In: Encyclopedia of renewable energy, sustainability and the environment. Amsterdam, The Netherlands: Elsevier; 2024. p. 591–604. doi:10.1016/b978-0-323-93940-9.00242-5.
4. Sharma P, Banerjee D. Biopolymers as solid polymer electrolytes: advances, challenges, and future prospects. Prabha Mater Sci Lett. 2025;4(2):128–47. doi:10.33889/pmsl.2025.4.2.012.
5. Chew KW, Ng TC, How ZH. Conductivity and microstructure study of PLA-based polymer electrolyte salted with lithium perchloride, $LiClO_4$. Int J Electrochem Sci. 2013;8(5):6354–64. doi:10.1016/s1452-3981(23)14767-5.
6. Osada I, Hosseini SM, Jeong S, Passerini S. Novel ternary polymer electrolytes based on poly(lactic acid) from sustainable sources. ChemElectroChem. 2017;4(3):463–7. doi:10.1002/celc.201600653.
7. Rayung M, Aung MM, Azhar SC, Abdullah LC, Su'ait MS, Ahmad A, et al. Bio-based polymer electrolytes for electrochemical devices: insight into the ionic conductivity performance. Materials. 2020;13(4):838. doi:10.3390/ma13040838.
8. Berradi A, Aziz F, El Achaby M, Ouazzani N, Mandi L. A comprehensive review of polysaccharide-based hydrogels as promising biomaterials. Polymers. 2023;15(13):2908. doi:10.3390/polym15132908.
9. Mudgil D, Barak S, Khatkar BS. Guar gum: processing, properties and food applications—a review. J Food Sci Technol. 2014;51(3):409–18. doi:10.1007/s13197-011-0522-x.
10. Musa TA, Ibrahim AF, Nasr-El-Din HA, Hassan AM. New insights into guar gum as environmentally friendly polymer for enhanced oil recovery in high-salinity and high-temperature sandstone reservoirs. J Petrol Explor Prod. 2021;11(4):1905–13. doi:10.1007/s13202-020-01080-3.

11. Venkatesh K, Jenova I, Shunmugavel K, Madeswaran S, Aristatil G, Gnanamuthu RM. Development of guar gum-based solid electrolyte for zinc-air battery applications. Polym Bull. 2025;82(18):12751–68. doi:10.1007/s00289-025-06043-4.
12. George A, Shah PA, Shrivastav PS. Guar gum: versatile natural polymer for drug delivery applications. Eur Polym J. 2019;112:722–35. doi:10.1016/j.eurpolymj.2018.10.042.
13. Giri P, Zandu SK, Singh I. Chemical modifications of guar gum for drug delivery applications: a review. Asian J Chem. 2020;32(6):1259–65. doi:10.14233/ajchem.2020.22607.
14. Ramamohan K, Achari VBS, Sharma AK, Lu X. Electrical and structural characterization of PVA/PEG polymer blend electrolyte films doped with $NaClO_4$. Ionics. 2015;21(5):1333–40. doi:10.1007/s11581-014-1302-1.
15. Fong KD, Self J, McCloskey BD, Persson KA. Ion correlations and their impact on transport in polymer-based electrolytes. Macromolecules. 2021;54(6):2575–91. doi:10.1021/acs.macromol.0c02545.
16. Ni'mah YL, Saputra MAE, Suprapto S, Fansuri H, Suwarta P, Subhan A, et al. The fabrication of solid polymer electrolyte from CS/PEO/$NaClO_4$/fly ash composite. Polymers. 2022;14(22):4792. doi:10.3390/polym14224792.
17. Cohen YS, Gabay Y, Cohen Y. Temperature-dependent impedance spectroscopy of molten alkali-halide salt binary mixtures. ECS Electrochem Lett. 2015;4(1):H1–4. doi:10.1149/2.0131501eel.
18. Kamisah MM, Siti Munirah H, Mansor MS. Electrochemical impedance study of lithium-ion insertion into rice husk carbon. Ionics. 2007;13(4):223–5. doi:10.1007/s11581-007-0095-x.
19. Ahmed MB, Nofal MM, Aziz SB, Al-Saeedi SI, Brza MA, Dannoun EMA, et al. The study of ion transport parameters associated with dissociated cation using EIS model in solid polymer electrolytes (SPEs) based on PVA host polymer: XRD, FTIR, and dielectric properties. Arab J Chem. 2022;15(11):104196. doi:10.1016/j.arabjc.2022.104196.
20. Aziz SB, Woo TJ, Kadir MFZ, Ahmed HM. A conceptual review on polymer electrolytes and ion transport models. J Sci Adv Mater Devices. 2018;3(1):1–17. doi:10.1016/j.jsamd.2018.01.002.
21. Chauhan S, Rawat S, Gupta S. Structural and electrical properties of composite doped cobalt ion conducting solid polymer electrolyte. Mater Today Proc. 2024;104:77–83. doi:10.1016/j.matpr.2024.02.015.
22. Jaipal Reddy M, Chu PP. Ion pair formation and its effect in PEO: Mg solid polymer electrolyte system. J Power Sources. 2002;109(2):340–6. doi:10.1016/S0378-7753(02)00084-8.
23. Teoh KH, Lim CS, Ramesh S. Lithium ion conduction in corn starch based solid polymer electrolytes. Measurement. 2014;48:87–95. doi:10.1016/j.measurement.2013.10.040.
24. Aziz SB, Ahmed MJ, Abdullah OG, Murad AR, Hamad SM, Hadi JM. Magnesium ion conducting biopolymer blend-based electrolyte for energy storage application: electrochemical characteristics. Electrochim Acta. 2023;461:142659. doi:10.1016/j.electacta.2023.142659.
25. Abdullah AM, Aziz SB, Brza MA, Saeed SR, Ali Al-Asbahi B, Sadiq NM, et al. Glycerol as an efficient plasticizer to increase the DC conductivity and improve the ion transport parameters in biopolymer based electrolytes: XRD, FTIR and EIS studies. Arab J Chem. 2022;15(6):103791. doi:10.1016/j.arabjc.2022.103791.
26. del Agua I, Mantione D, Casado N, Sanchez-Sanchez A, Malliaras GG, Mecerreyes D. Conducting polymer iongels based on PEDOT and guar gum. ACS Macro Lett. 2017;6(4):473–8. doi:10.1021/acsmacrolett.7b00104.
27. Singh AV, Kumawat IK. Synthesis and characterization of a new guar gum 4-hydroxybenzoic acid resin and its use for the separation of heavy metal ions in industrial effluents. Polym Eng Sci. 2013;53(3):546–54. doi:10.1002/pen.23294.
28. Khurshid A, Bajaj Y, Savilov SV, Yadav T, Kumar R, Yahya MZA, et al. MXene nanofiller doped ion conducting polyethylene oxide for electrochemical devices. Energy Storage. 2024;6:e563. doi:10.1002/est2.563.
29. Dhumal S, Patil A, Jadhav NA, Saxena A, Dighavkar C. Synthesis characterization and dielectric properties of PVA/F 127 block copolymer blend polymer electrolyte for PSSC application. Int J Emerg Technol Innov Res. 2023;10(7):f449–60.
30. Lee TK, Afiqah S, Ahmad A, Dahlan HM, Rahman MYA. Temperature dependence of the conductivity of plasticized poly(vinyl chloride)-low molecular weight liquid 50% epoxidized natural rubber solid polymer electrolyte. J Solid State Electrochem. 2012;16(6):2251–60. doi:10.1007/s10008-011-1633-z.

31. Ahmad NH, Nizam MI, Isa M, Ahmad NH, Isa MIN. Ionic conductivity and electrical properties of carboxymethyl cellulose-NH_4Cl solid polymer electrolytes. J Eng Sci Technol. 2016;11(8):839–47.
32. Abdulkadir BA, Dennis JO, Bin Abd Shukur MF, Nasef MME, Usman F. Study on dielectric properties of gel polymer electrolyte based on PVA-K_2CO_3 composites. Int J Electrochem Sci. 2021;16(1):150296. doi:10.20964/2021.01.34.
33. Fadzallah IA, Majid SR, Careem MA, Arof AK. Relaxation process in chitosan–oxalic acid solid polymer electrolytes. Ionics. 2014;20(7):969–75. doi:10.1007/s11581-013-1058-z.
34. Gökçen M, Altuntaş H. On the profile of temperature dependent electrical and dielectric properties of Au/SiO_2/n-GaAs (MOS) structures at various frequencies. Phys B Condens Matter. 2009;404(21):4221–4. doi:10.1016/j.physb.2009.08.023.
35. Kaya A, Vural Ö, Tecimer H, Demirezen S, Altındal Ş. Frequency and voltage dependence of dielectric properties and electric modulus in Au/PVC + TCNQ/p-Si structure at room temperature. Curr Appl Phys. 2014;14(3):322–30. doi:10.1016/j.cap.2013.12.005.
36. Rayssi C, El Kossi S, Dhahri J, Khirouni K. Frequency and temperature-dependence of dielectric permittivity and electric modulus studies of the solid solution $Ca_{0.85}Er_{0.1}Ti_{1-x}Co_{4x/3}O_3$ ($0 \le x \le 0.1$). RSC Adv. 2018;8(31):17139–50. doi:10.1039/c8ra00794b.
37. Karmakar A, Ghosh A. Dielectric permittivity and electric modulus of polyethylene oxide (PEO)–$LiClO_4$ composite electrolytes. Curr Appl Phys. 2012;12(2):539–43. doi:10.1016/j.cap.2011.08.017.
38. Lundin F, Aguilera L, Hansen HW, Lages S, Labrador A, Niss K, et al. Structure and dynamics of highly concentrated LiTFSI/acetonitrile electrolytes. Phys Chem Chem Phys. 2021;23(25):13819–26. doi:10.1039/d1cp02006d.
39. Pal P, Ghosh A. Investigation of ionic conductivity and relaxation in plasticized PMMA-$LiClO_4$ solid polymer electrolytes. Solid State Ion. 2018;319:117–24. doi:10.1016/j.ssi.2018.02.009.
40. Kumar M, Tiwari T, Kumar Chauhan J, Srivastava N. Understanding the ion dynamics and relaxation behavior from impedance spectroscopy of NaI doped Zwitterionic polymer system. Mater Res Express. 2014;1(4):045003. doi:10.1088/2053-1591/1/4/045003.
41. Ravi M, Bhavani S, Pavani Y, Narasimha Rao VVR. Investigation on electrical and dielectric properties of PVP: $KCLO_4$ polymer electrolyte films. Indian J Pure Appl Phys. 2013;51(5):362–6. doi:10.1016/j.matchemphys.2011.07.006.
42. Srivastava N, Kumar M. Ion dynamics and relaxation behavior of $NaPF_6$-doped polymer electrolyte systems. J Solid State Electrochem. 2016;20(5):1421–8. doi:10.1007/s10008-016-3147-1.
43. Mohd Bahaudin Bokhari NMB, Sohaimy MIH, Isa MINM. Structural investigation of solid biopolymer electrolytes: 2-hydroxyethyl cellulose doped ammonium formate as a promising proton conductor. Adv Manuf Polym Compos Sci. 2024;10(1):2335850. doi:10.1080/20550340.2024.2335850.
44. Shahid M, Bukhari SA, Gul Y, Munir H, Anjum F, Zuber M, et al. Graft polymerization of guar gum with acryl amide irradiated by microwaves for colonic drug delivery. Int J Biol Macromol. 2013;62:172–9. doi:10.1016/j.ijbiomac.2013.08.018.
45. Cyriac V, Ismayil, Noor IM, Mishra K, Chavan C, Bhajantri RF, et al. Ionic conductivity enhancement of PVA: carboxymethyl cellulose poly-blend electrolyte films through the doping of NaI salt. Cellulose. 2022;29(6):3271–91. doi:10.1007/s10570-022-04483-z.
46. Li Z, Fu J, Zhou X, Gui S, Wei L, Yang H, et al. Ionic conduction in polymer-based solid electrolytes. Adv Sci. 2023;10(10):2201718. doi:10.1002/advs.202201718.
47. Jain V, Tammishetti V, Joshi K, Kumar D, Pradip, Rai B. Guar gum as a selective flocculant for the beneficiation of alumina rich iron ore slimes: density functional theory and experimental studies. Miner Eng. 2017;109:144–52. doi:10.1016/j.mineng.2017.03.007.
48. Boshoman SB, Fatoba OS. Data pertaining to the catalytic capabilities of transition metal oxides for fuel cell applications. Data Brief. 2024;57:110988. doi:10.1016/j.dib.2024.110988.
49. Kohn W, Sham LJ. Self-consistent equations including exchange and correlation effects. Phys Rev. 1965;140(4A):A1133–8. doi:10.1103/physrev.140.a1133.
50. Bruce PG, Vincent CA. Polymer electrolytes. Faraday Trans. 1993;89(17):3187. doi:10.1039/ft9938903187.

51. McNeill IC. Polymer electrolyte reviews—1. Polym Degrad Stab. 1988;20(1):89. doi:10.1016/0141-3910(88)90096-1.
52. Mostefai A. Charge density and density of states (DOS) of monoclinic ZrO_2 using meta-GGA DFT functional. J Nano-Electron Phys. 2022;14(3):03026. doi:10.21272/jnep.14(3).03026.
53. Aryanpour A, Sadeghi A. Machine learning the local electronic density of states. arXiv:2504.16052. 2025.
54. Bin How W, Chong S, Grasselli F, Huguenin-Dumittan KK, Ceriotti M. Adaptive energy reference for machine-learning models of the electronic density of states. Phys Rev Mater. 2025;9:013802. doi:10.1103/physrevmaterials.9.013802.
55. Kazachenko AS, Akman F, Sagaama A, Issaoui N, Malyar YN, Vasilieva NY, et al. Theoretical and experimental study of guar gum sulfation. J Mol Model. 2021;27:5. doi:10.1007/s00894-020-04645-5.